

# 20Gb/s Silicon Ring Modulator Co-Integrated with a Ge Monitor Photodetector

M. Pantouvaki<sup>(1)</sup>, P. Verheyen<sup>(1)</sup>, G. Lepage<sup>(1)</sup>, J. De Coster<sup>(1)</sup>, H. Yu<sup>(2)</sup>, P. De Heyn<sup>(2)</sup>, P. Absil<sup>(1)</sup> and J. Van Campenhout<sup>(1)</sup>

<sup>(1)</sup> Imec, Kapeldreef 75, B-3001 Leuven, Belgium, (Marianna.Pantouvaki@imec.be)

<sup>(2)</sup> Department of Information Technology, Ghent University – imec, Center of Nano- and Biophotonics, St. Pietersnieuwstraat 41, 9000 Ghent, Belgium

**Abstract** We demonstrate the monolithic integration of a 20Gb/s silicon ring modulator with low dark-current Ge monitor photodetectors. The wavelength exhibiting optimum modulation performance can be tracked by measuring the photocurrent of monitor photodetectors implemented at the through and drop port of the ring modulator.

## Introduction

The recent increase of cloud computing and internet traffic as well as the interconnect bottleneck in high performance multi-processors have raised interest in developing more cost-effective high bandwidth-density optical transmitters and receivers. Silicon photonics technology is attractive towards this goal because it can re-use existing CMOS fabrication equipment and integration processes for optimum yield and for high volume manufacturing. The monolithic integration of silicon modulators with photodetectors in particular enables large density and high bandwidth optical transceivers. Co-integration of silicon Mach-Zehnder modulators with Ge photodetectors was recently demonstrated for operation up to 30Gb/s<sup>1,2</sup>.

Silicon ring modulators are interesting for wavelength-division-multiplexed systems, because they can reduce the footprint and the energy consumption of the transmitter<sup>3</sup>. However, the high thermo-optic coefficient of the silicon and the narrow optical bandwidth of the ring resonance make such modulators sensitive to temperature variations. Thermal control of

ring modulators via a dynamic feedback loop has been proposed to solve this problem<sup>4,5</sup>. Such a feedback loop would require monitoring either the temperature or the power in the ring before providing feedback to a control circuit.

In this paper we demonstrate a silicon ring modulator monolithically integrated with Ge photodetectors for monitoring the power inside the ring and therefore detecting wavelength shifts due to temperature drift. Dynamic operation of the ring modulator is demonstrated at 20Gb/s. At 0.25mW optical power at the input port of the ring, photocurrents of  $\sim 5\mu\text{A}$  and  $\sim 15\mu\text{A}$  are measured in detectors implemented in the through and drop port respectively, at optimum operation point of the modulator.

## Device fabrication

The silicon ring modulators and Ge photodetectors were fabricated on 200mm silicon-on-insulator (SOI) wafers with 220nm thick silicon and 2 $\mu\text{m}$  thick buried oxide. Large ring modulators of 40 $\mu\text{m}$  ring radius were formed by etching 70nm of the crystalline silicon, followed by oxide deposition, planarization and lithography to define the doping areas of the p-n junction parallel to the

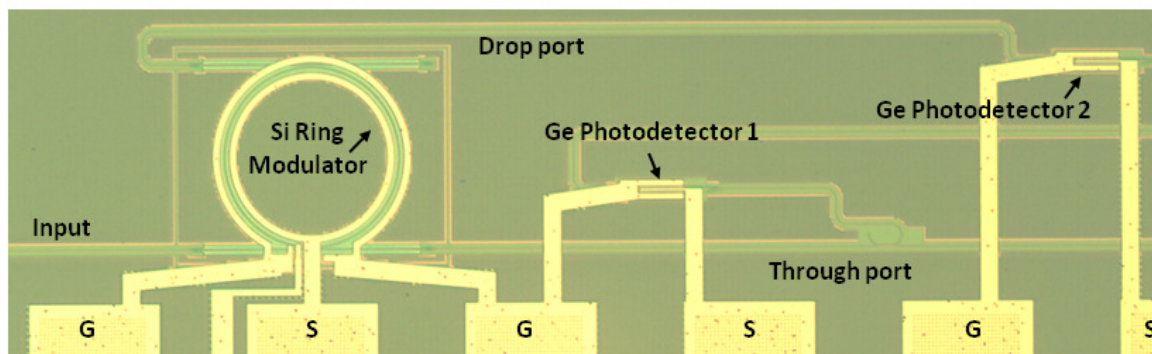


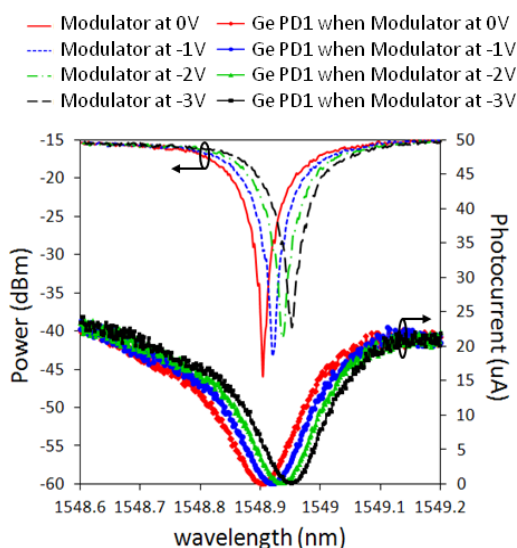
**Fig. 1:** Microscope image of the silicon micro-ring modulator co-integrated with two Ge photodetectors.

ring waveguide. High-dose contact areas were formed  $\sim 2\mu\text{m}$  away from the ring waveguide. After implantation and rapid thermal annealing at  $\sim 1000^\circ\text{C}$ , a poly-silicon layer was deposited, annealed, patterned and planarised before the Ge epitaxial growth. The Ge module included epitaxial growth of Ge on the crystalline silicon, Ge annealing at  $850^\circ\text{C}$ , Ge chemical-mechanical polishing (CMP), doping and annealing at  $550^\circ\text{C}$ . On top of the active devices a thick pre-metal-dielectric was deposited. This was followed by standard 130nm CMOS interconnect technology processing to form W-contacts and Cu-metal lines for contacting the modulators and the photodetectors. More processing details can be found in <sup>2,6</sup>.

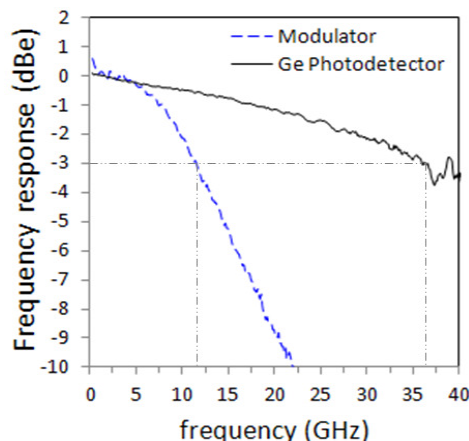
### Experimental results

Fig. 1 shows a microscope picture of the final silicon ring modulator with a bus waveguide and a drop port. In this design, identical Ge photodetectors based on vertical p-i-n junctions of  $20\mu\text{m}$  length were placed at the drop (Ge PD2) and through (Ge PD1) ports. The measured responsivity of these devices was  $\sim 0.37\text{A/W}$  at  $1550\text{nm}$  and the dark current was  $\sim 28\text{nA}$  at  $-1.2\text{V}$ . At the through port, optical power was coupled into the photodetector via a  $\sim 20\%$  coupler. The gap between the bus waveguide and the ring was  $570\text{nm}$ , while the gap between the ring and the drop port was  $800\text{nm}$ . The goal of this design was to achieve approximately the same maximum photocurrent on the two Ge photodetectors.

Typical transmission spectra of the silicon ring modulator are shown in Fig. 2. The Q-factor



**Fig. 2:** Typical transmission spectra of the ring modulator at different bias, and photocurrent response of Ge PD1 to varying modulator bias. The Ge PD1 bias was fixed to  $-1.2\text{V}$ .



**Fig. 3:** Frequency response of ring modulator at  $0\text{V}$  bias and of Ge PD1 at  $-1\text{V}$  bias.

of this device was  $\sim 11000$ , while the modulation efficiency was  $18\text{pm/V}$  for a voltage shift from  $0\text{V}$  to  $-1\text{V}$ . The photocurrent measured on Ge photodetector 1 is also shown in Fig. 2 for a fixed photodetector bias of  $-1.2\text{V}$  and  $\sim 0.25\text{mW}$  optical power at the ring input port. The photocurrent varies between  $0.1\mu\text{A}$  and  $20\mu\text{A}$ , and the minimum follows the wavelength shift of the silicon modulator resonance as the applied bias on the modulator is changing. This shows that the photodetector current can be used for monitoring resonance shifts at the modulator, which can be caused either by voltage changes or by temperature fluctuations.

The small-signal frequency response of the co-integrated devices was measured on a network analyser using  $-5\text{dBm}$  RF input power. Fig. 3 shows the results from the modulator and the Ge photodetector at the through port. The frequency response of the modulator at  $0\text{V}$  was  $\sim 11.5\text{GHz}$ , limited by the device capacitance and the  $50\Omega$  drive impedance. The Ge photodetector had a 3-dB bandwidth of  $36\text{GHz}$  at  $-1.2\text{V}$  bias.

From the DC measurements, the transmitter penalty (TP) can be calculated for a given voltage swing as

$$TP[\text{dB}] = -10 \log_{10} \left( \frac{P_1 - P_0}{2P_{in}} \right)$$

where  $P_1$ ,  $P_0$  and  $P_{in}$  are the power transmitted during a 1-bit, a 0-bit and the input power, respectively. The best operating point of a modulator occurs at minimum transmitter penalty, which implies the best combination of extinction ratio and insertion loss.

Fig. 4 shows the transmitter penalty of the ring modulator, calculated for a voltage swing from  $0\text{V}$  to  $-1\text{V}$ , plotted together with the photocurrent measured on the Ge photodetectors 1 and 2. The photodetector bias was fixed to  $-1.2\text{V}$  for

this measurement. As expected, the minimum photocurrent on Ge PD1 coincides with the maximum photocurrent on Ge PD2. But minimum transmitter penalty does not correspond to the wavelength of minimum or maximum photocurrent. There is a region around the minimum transmitter penalty where there is photocurrent measured by both photodetectors. Variations in the photocurrent of one or both of these photodetectors can be used in a feedback loop for monitoring the wavelength drift of the ring modulator. In one approach, the feedback loop could monitor current change in Ge PD1 (or PD2) and stabilize the current to the value corresponding to minimum transmitter penalty. In another approach, the feedback signal could be based on the difference of the photocurrents in the two Ge photodetectors.

The silicon ring modulator was tested at 20Gb/s using a PRBS signal of  $2^{15}-1$ . Optical eye diagrams at different wavelengths are also shown in Fig. 4, using 2V peak-to-peak swing (measured at the input of the probe) and -2.5V bias on the modulator. Optimum eye diagrams occur at wavelengths where both photodetectors exhibit photocurrent. Dynamic extinction ratios of 3.5dB and 4.5dB were measured at points B and E in Fig. 4, corresponding to photocurrent values of  $\sim 5\mu\text{A}$  and  $\sim 15\mu\text{A}$  for Ge PD1 and Ge PD2 respectively. Such current levels are sufficiently high to feed into an optimized feedback control circuit.

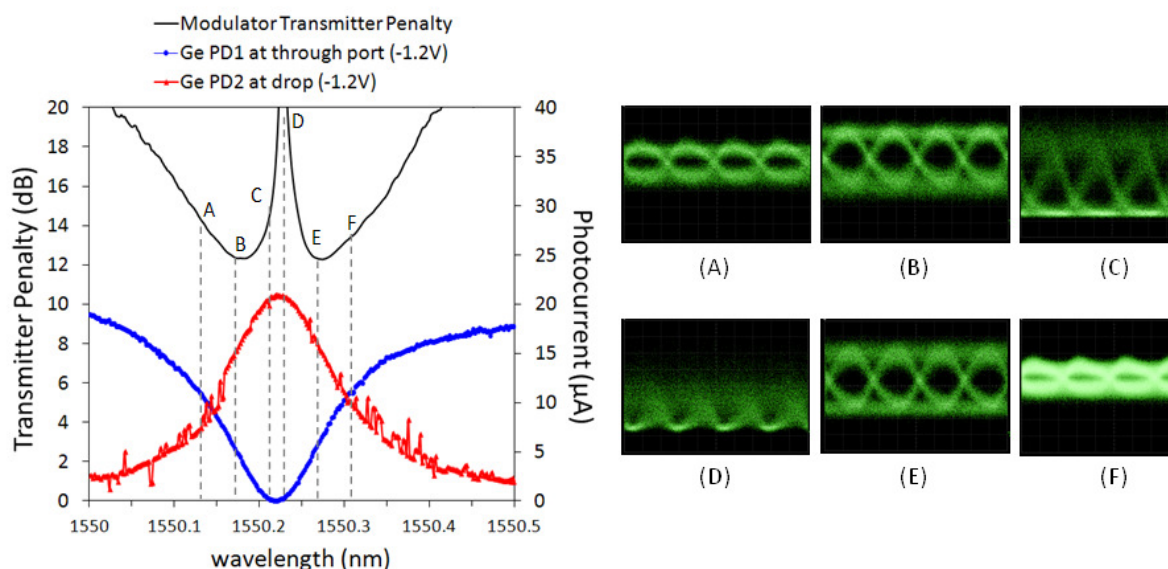


**Fig. 4:** Transmitter penalty of silicon ring modulator and photocurrent spectra measured on Ge PD1 and Ge PD2. The bias of the modulator and the photodetectors was set to 0V and -1.2V respectively. Eye diagrams at 20Gb/s are also shown at different wavelengths.

## Conclusions

The co-integration of a silicon ring modulator with Ge photodetectors was demonstrated on the same wafer, enabling integrated monitoring of the power in the ring modulator. The modulation efficiency of the ring with drop port was 18pm/V. Best eye diagrams at 20Gb/s, demonstrating dynamic extinction ratios of 3.5-4.5dB, were measured at the same wavelengths where photocurrents of  $\sim 10\mu\text{A}$  were measured in the monitoring photodetectors for 0.25mW optical input power. Optimization of the coupling design and the detector responsivity can further enhance the monitor currents, enabling a low-power feedback control loop.

## Acknowledgements

The authors acknowledge imec's 200mm pline for contributions to the device fabrication. This work was supported by imec's Core Partner Program.

## References

- [1] G. Kim et al., Optics Express **19**, 26936, (2011).
- [2] P. Verheyen et al., Proc. SPIE **8431**, 843114 (2012).
- [3] M. Rakowski et al, OFC Conf. OM2H (2013).
- [4] K. Padmaraju et al, Optics Express **20**, 27999 (2012).
- [5] A. L. Lentine et al, Opt. Interconnect Conf., 46 (2012).
- [6] M. Pantouvaki et al, IEEE J. Selected Topics in Quant. Electron. **19** (2), 7900308 (2013).